



Crustal Architecture of the Cascadia Forearc

A. M. Trehu; I. Asudeh; T. M. Brocher; J. H. Luetgert; W. D. Mooney; J. L. Nabelek; Y. Nakamura

Science, New Series, Vol. 266, No. 5183. (Oct. 14, 1994), pp. 237-243.

Stable URL:

<http://links.jstor.org/sici?sici=0036-8075%2819941014%293%3A266%3A5183%3C237%3ACAOTCF%3E2.0.CO%3B2-S>

Science is currently published by American Association for the Advancement of Science.

Your use of the JSTOR archive indicates your acceptance of JSTOR's Terms and Conditions of Use, available at <http://www.jstor.org/about/terms.html>. JSTOR's Terms and Conditions of Use provides, in part, that unless you have obtained prior permission, you may not download an entire issue of a journal or multiple copies of articles, and you may use content in the JSTOR archive only for your personal, non-commercial use.

Please contact the publisher regarding any further use of this work. Publisher contact information may be obtained at <http://www.jstor.org/journals/aaas.html>.

Each copy of any part of a JSTOR transmission must contain the same copyright notice that appears on the screen or printed page of such transmission.

The JSTOR Archive is a trusted digital repository providing for long-term preservation and access to leading academic journals and scholarly literature from around the world. The Archive is supported by libraries, scholarly societies, publishers, and foundations. It is an initiative of JSTOR, a not-for-profit organization with a mission to help the scholarly community take advantage of advances in technology. For more information regarding JSTOR, please contact support@jstor.org.

Crustal Architecture of the Cascadia Forearc

A. M. Trehu,* I. Asudeh, T. M. Brocher, J. H. Luetgert, W. D. Mooney, J. L. Nabelek, Y. Nakamura

Seismic profiling data indicate that the thickness of an accreted oceanic terrane of Paleocene and early Eocene age, which forms the basement of much of the forearc beneath western Oregon and Washington, varies by approximately a factor of 4 along the strike of the Cascadia subduction zone. Beneath the Oregon Coast Range, the accreted terrane is 25 to 35 kilometers thick, whereas offshore Vancouver Island it is about 6 kilometers thick. These variations are correlated with variations in arc magmatism, forearc seismicity, and long-term forearc deformation. It is suggested that the strength of the forearc crust increases as the thickness of the accreted terrane increases and that the geometry of the seaward edge of this terrane influences deformation within the subduction complex and controls the amount of sediment that is deeply subducted.

The active and dormant volcanoes of the High Cascades (Fig. 1) are part of a volcanic arc that extends from southern Vancouver Island, Canada, to northern California. The presence of this arc indicates that oceanic lithosphere is being subducted beneath the North American continent. This interpretation is confirmed by the presence of a well-defined deformation front offshore, which is formed as the flat-lying sediments deposited in the oceanic basin are deformed as they are scraped off of the subducting Juan de Fuca and Gorda plates (Fig. 1) and accreted to the overriding North American plate (1). Although this region, generally known as the Cascadia subduction zone, is similar in many respects to other subduction zones, the rate of both upper and lower plate seismicity is much lower than is generally found in such tectonic settings (2). However, damaging earthquakes in northern California in 1992 and in Oregon in 1993, reveal the potential for significant seismic activity in this region. Results of several geologic studies, moreover, suggest that the region may have been affected by several large prehistoric earthquakes, the most recent having occurred approximately 300 years ago (3).

Because of this poorly defined but potentially great seismic hazard, many geophysical studies have been conducted in the past decade to characterize the lithospheric structure associated with this system in order to detect differences between this system and other, more typical, sub-

duction zones. Tomographic studies of mantle velocity structure have shown that a high-velocity subducted lithospheric slab similar to that found beneath other volcanic arcs is present in the upper mantle beneath western Washington and Oregon (4). Thermal modeling suggests that the low level of seismicity along the plate interface may be due in part to the young age of the subducted lithosphere, the relatively slow convergence rate between the North American and Juan de Fuca plates, and the high regional sedimentation rate (5). However, uncertainties in both the thermal and mantle velocity models are associated with uncertainties in forearc crustal structure and the position of the plate boundary, which was well known only beneath southwestern Canada before the studies reported here (6).

To determine whether crustal structure might, in part, be responsible for the apparently anomalous seismicity associated with Cascadia subduction, we conducted seismic experiments in 1989, 1991, and 1993 to image the crustal architecture of the forearc beneath northwestern Oregon and southwestern Washington (Fig. 1). Details of the data acquisition, processing, and modeling are discussed in (7) and (8). In this article, we use data from these experiments to construct an east-west crustal velocity model that extends from the abyssal plain seaward of the deformation front to the Cascades arc of central Oregon, and a model that extends from south to north along the boundary between the Willamette Valley and the Oregon Coast Range and into the Coast Range of southwest Washington.

Geologic Setting

The basement rocks throughout much of the Cascadia forearc (that is, the region between the deformation front and the High Cascades) in northwestern Oregon

and southwestern Washington are generally thought to be Paleocene and early Eocene in age (50 to 60 million years old) and represent oceanic crust and seamounts that were accreted to North America approximately 50 Ma (million years ago). These rocks crop out in anticlines in the Coast Range and have been drilled in several places beneath the Willamette Valley and the Oregon continental shelf. Although they are known locally by a variety of names (9), we refer to them collectively as the Siletz terrane. Their origin is uncertain. Suggested possibilities include an island chain formed above a hot spot near the Farallon-Kula spreading plate boundary (10) and formation by oblique rifting of a continental margin (11).

The location of the western boundary of the Siletz terrane can be mapped with seismic reflection and magnetic anomaly data offshore and geologic observations onshore (12). The eastern boundary is hidden by the thick sediments of the Willamette and Puget Sound basins or by the volcanic rocks of the Cascades (13, 14). The northern and southern ends of the Cascadia forearc are floored by rocks of pre-Tertiary age (greater than 66 million years old), which represent the amalgamation of many different terranes.

Between the western edge of the Siletz terrane and the deformation front is the subduction complex, formed by progressive addition of sediments and fragments of oceanic crust to the continental edge. The subduction complex is exposed onshore on the Olympic peninsula in northwestern Washington and in the Eel River basin of northern California. A major objective of our study was to contrast the crustal structure in a region where most of the forearc is floored by the Siletz terrane to the structure further north, where the forearc records a longer geologic history.

North-South Cross Section

The data overall reveal that the crust is made up of several layers that vary in thickness from north to south and from east to west. Along the NS (north-south) profile (Fig. 2), large lateral velocity variations in the upper 2.5 km correlate well with known sedimentary basins (velocity 2 to 4 km/s) and basement uplifts (velocity 4 to 5 km/s). These velocity variations are manifested in the data by oscillations in the observed time of Pg arrivals (Fig. 2, insert, and Fig. 3). Below a depth of 2.5

A. M. Trehu and J. L. Nabelek are in the Department of Oceanic and Atmospheric Sciences, Oceanography Administration Building 104, Oregon State University, Corvallis, OR 97331, USA. I. Asudeh is at the Geological Survey of Canada, 1 Observatory Crescent, Ottawa, Ontario, Canada K1A 0Y3. T. M. Brocher, J. H. Luetgert, and W. D. Mooney are at the U.S. Geological Survey, 345 Middlefield Road, Menlo Park, CA 94025, USA. Y. Nakamura is at the Institute for Geophysics, University of Texas, 8701 North Mopac Boulevard, Austin, TX 78759, USA.

* To whom correspondence should be addressed.

km, lateral velocity variations are smaller, suggesting that the basins are shallow and are underlain by the same high-velocity material that comprises the basement uplifts. Basement velocities increase with depth and reach 6.5 km/s at a depth of 11 km south of model km 175 and at a depth of 7 km north of model km 100. We estimate the uncertainty in the depth to the 6.5-km/s contour to be less than 1 km (7).

Because of the high velocity at shallow depth, no Pg arrivals are observed from the lower crust in spite of the maximum recorded offset of 350 km. Information on the total crustal thickness and on the average velocity of the lower crust was obtained from wide-angle reflections that are observed as secondary arrivals and modeled as reflections from the crust-mantle interface (PmP on Fig. 2, insert, and Fig. 3). Systematic differences in the amplitude of these wide-angle reflections as a function of shot-receiver offset indicate

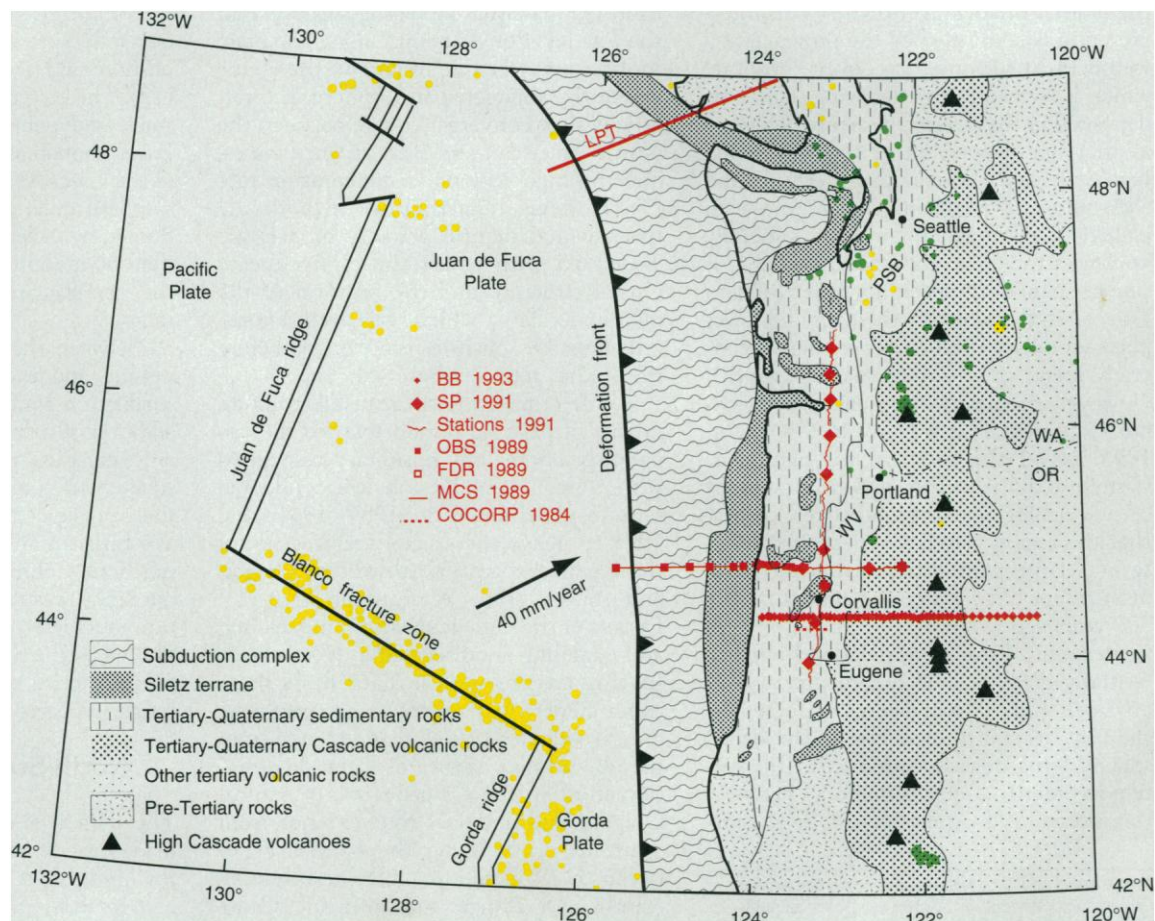
that the average velocity of the lower crust varies along the profile from 6.5 to 7.2 km/s (7). Inversion of the observed travel times of the wide-angle reflections for several possible lower crustal velocity models indicates that the crust is 45 to 50 km thick beneath the central 150 km of the profile. This estimate is somewhat larger than, but generally consistent with, an independent estimate of 40 to 43 km beneath Corvallis obtained from analysis of teleseismic receiver functions (15).

The velocity structure of the upper 25 km of the crust is strikingly similar to that of the 36-km-thick Ontong Java Plateau (16), which is thought to be the marine equivalent of a continental flood basalt. Many studies show that the thickness of the upper part of the oceanic crust, as defined by velocities less than 6.5 km/s, increases as the total oceanic crustal thickness increases, both for normal oceanic crust and for the anomalously thick oceanic crust found be-

neath volcanic passive margins and oceanic plateaus (16). Therefore, we interpret the 6.5-km/s isovelocity contour to be the base of the upper crust of the Siletz terrane. Our model indicates northward thinning of the upper crust, suggesting that the total thickness of the Siletz terrane also decreases to the north.

The total crustal thickness of 45 to 50 km is considerably greater than the inferred thickness of the Siletz terrane. We interpret the lowermost 5 to 8 km of the crust to be oceanic crust of the subducted Juan de Fuca plate, implying that the North American–Juan de Fuca plate boundary lies within the lower crust and that the Oregon Coast Range and western Willamette Valley are underlain by lithospheric upper mantle of the Juan de Fuca plate (17). The region between the inferred base of the Siletz terrane and the top of the Juan de Fuca plate is laterally heterogeneous and may comprise variable amounts of tectonically under-

Fig. 1. Locations of the 1989 and 1991 active-source seismic experiments and 1993 passive-source broadband seismic array overlain on a simplified geologic map of the United States Pacific Northwest region [with information from (11) onshore and from (12) offshore]. Plate boundaries offshore are also shown. The relative motion vector between the Juan de Fuca and North American plates is from the global plate model of C. DeMets *et al.* (41). The Siletz terrane [as defined in (9)] is shown onshore only where it is exposed at the surface; its offshore extent is derived from multichannel seismic reflection and magnetic data. The line labeled LPT indicates the location of a similar transect across the forearc in southwestern Canada (5), and the short dashed east-west line (COCORP 1984) between Corvallis and Eugene shows the location of the only deep-crustal seismic reflection profile onshore in this region (16). Offshore, earthquake epicenters are shown in yellow; most are shallow and are associated with the Blanco fracture zone. Onshore, earthquakes with hypocenters shallower than 45 km are shown in green and are assumed to be in the North American plate; earthquakes with hypocenters deeper than 45 km are shown in yellow and are assumed to be in the Juan de Fuca plate. Hypocenters east of 126°W are from the database published by the University of Washington seismic network and include events occurring between February 1969 and



February 1994. West of 126°W, epicenters are from the Preliminary Determination of Epicenters (PDE) database distributed by the U.S. Geological Survey. This distribution of seismicity is characteristic of the historical seismicity of the Pacific Northwest. Not shown on this map is a second region of active seismicity associated with the Cascadia subduction zone in northwestern California near Cape Mendocino. SP, shot point; OBS, ocean bottom seismometer; FDR, 5-day recorder; MCS, multichannel seismic; BB, broadband seismic station; WV, Willamette Valley; PSB, Puget Sound basin.

plated oceanic crust, magmatically underplated mafic material, and serpentinized North American upper mantle (18).

East-West Cross Section

The east-west velocity variations indicated by our seismic data (Fig. 4) contrast significantly with several published summaries of

the crustal structure of western Oregon (19). These summaries were based on earlier models of seismic and gravity data and showed a 15- to 20-km-thick crust beneath the Coast Range underlain in some models by the upper mantle of the North American plate and in others by upper mantle of the Juan de Fuca plate. Our model, however, is consistent with a coincident model of the

electrical conductivity of the crust and upper mantle (20).

A well-defined deformation front is observed in the sediments approximately 100 km west of the coast (model km 30) and marks the seaward edge of the Cascadia subduction zone (21). East of the deformation front (km 30 to 100) is a zone of highly deformed sediments we refer to as the subduction complex. Model velocities in this region likely are a smoothed representation of a structure consisting of blocks of high-velocity material embedded in a low-velocity matrix, as is typical of subduction complexes exposed on land. Although the subducted oceanic crust cannot be traced more than 30 km east of the deformation front in the multichannel reflection data, the large-aperture data require that it underlies the entire continental margin (22).

On the continental shelf, a block-faulted basement surface that represents the top of the Siletz terrane underlies a 5-km-thick sedimentary basin. The sediments in this basin record a complicated Neogene history of folding, faulting, uplift, subsidence, and magmatic intrusion (12). Our model indicates that the Siletz terrane is at least 10 km thick beneath the basin and forms a steeply dipping ($>50^\circ$) subduction backstop (23), as interpreted from the abrupt eastward increase in mid-crustal velocity 35 km west of the coast (model km 105). This geometry is well constrained by Pg arrivals recorded on onshore stations from offshore shots and by preliminary modeling of magnetic anomalies and supports an earlier inference, based primarily on seismic reflection and magnetic data, of a steeply dipping crustal boundary in this region (24). A fault that cuts the entire sedimentary section overlying the seaward edge of the Siletz terrane is observed in the seismic reflection data (6) and suggests that this crustal boundary is localizing current forearc deformation. A subhorizontal reflection beneath the shelf originates at a depth of about 17 km and probably indicates either the base of the Siletz or the top of subducting oceanic crust (6, 7). In the absence of large-aperture data, this reflection would probably have been interpreted as the base of the crust, yielding an estimate of crustal thickness that was consistent with earlier studies. However, wide-angle reflections from the base of the crust indicate that the crustal thickness increases from about 22 km beneath the outer continental shelf to 30 km beneath the coast.

Onshore, our model indicates that the 2-km-thick layer of low-velocity material beneath the Willamette Valley extends about 30 km east of the surface occurrence of the volcanic rocks of the western Cascades. This relation suggests that the western Cascade rocks were erupted over a well-developed sedimentary basin (25). Material

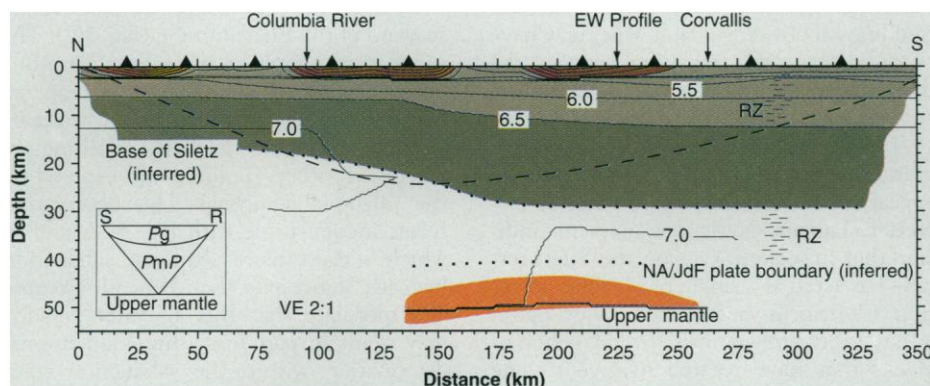


Fig. 2. Velocity model of the crust beneath the NS (north-south) profile. The insert illustrates the seismic ray paths discussed in the text (S, source; R, receiver). Isovelocity contours are labeled in units of kilometers per second, and the contour interval is 0.5 km/s. Triangles show shot point positions. Recording stations were at 750-m intervals along the profile. The portion of the model constrained by Pg observations is shown by a dashed line; velocities above this line are generally constrained to approximately -0.1 km/s. The root-mean-square (rms) misfit of the model to the observed Pg travel times for all nine shot points is 0.10 s. The brown shaded regions are sedimentary basins in which the velocity increases from 2 to 4 km/s. Our interpretation of the upper and lower crust of the Siletz terrane is shown in light and dark green, respectively. The position of the base of the crust derived from travel times of wide-angle reflections (PmP) for one possible model is shown as a double line. The orange shaded region at the base of the crust illustrates the allowable range of crustal thickness and is bounded on the top by the solution assuming a lower crustal velocity of 6.5 km/s and bounded on the bottom by a solution assuming a lower crustal velocity of 7.2 km/s. The inferred positions of the base of the Siletz terrane and of the North American–Juan de Fuca (NA/JdF) plate boundary are discussed in the text and contain uncertainties qualitatively estimated to be on the order of 6 km. Reflective zones labeled RZ are from (18).

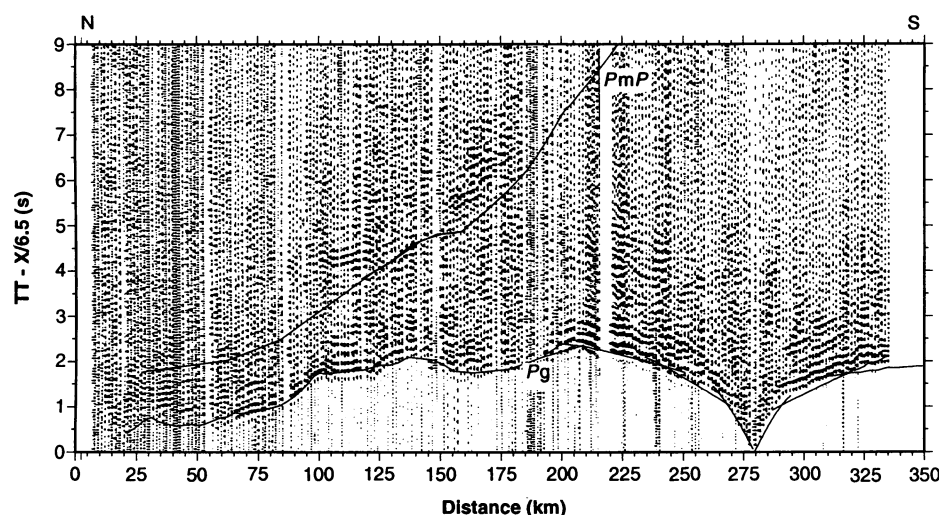


Fig. 3. One of the nine shot gathers from which the model of Fig. 2 was constructed. Two adjacent traces were added together, and data were filtered with a passband of 5 to 20 Hz for this display. The y axis represents time after the shot reduced by a factor of $X/(6.5 \text{ km/s})$, where X is source–receiver offset in kilometers. Travel times predicted by the model of Fig. 2 for Pg and PmP arrivals are overlain on the data. The rms misfit of the model to the Pg observations is 0.10 s (the same as for the entire data set). Undulations in the travel times result from large, shallow velocity variation. The transition to an apparent velocity greater than 6.5 km/s is observed in this shot gather at km 205. The lateral variation in the depth to this velocity transition is well constrained by the distribution of shot gathers along the profile (Fig. 2).

with a velocity appropriate for Siletz basement underlies the entire valley. Although our data do not constrain the eastward extent of the Siletz terrane, gravity data indicate that the high-velocity material at shallow depth at the eastern end of our model corresponds to a local magmatic intrusion rather than to a major terrane boundary. Lower densities (14) and velocities (26) at upper and mid-crustal levels beneath the High Cascades suggest that the eastern boundary of the Siletz block occurs beneath the western Cascades.

The geometry of the base of the subducted Juan de Fuca crust, as extrapolated from the coast to the NS profile, implies a plate dip of about 13° to 16° beneath the Coast Range, significantly less than the 20° dip assumed in models that postulate a pronounced arch in the subducted plate beneath the Olympic mountains (27), but consistent with the dip obtained from modeling the teleseismic receiver function beneath Corvallis, Oregon (15).

Discussion

Although the dip of the subducted Juan de Fuca plate beneath central Oregon (Fig. 5A) is similar to that beneath southwestern Canada (Fig. 5B), the structure within the overlying wedge of North American plate crust is significantly different. The velocity and inferred thickness of the Siletz terrane beneath northwestern Oregon suggest a vigorous magmatic source (28), supporting suggestions that these rocks may represent the initial stage of volcanism associated with the Yellowstone hot spot (10, 11). Beneath British Columbia, where the Siletz terrane (9) does not crop out onshore but is recognized in the subsurface offshore through correlation of drilling results with seismic profiling, it appears to be oceanic crust of approximately normal thickness (6). We interpret the northward thinning of the Siletz terrane to represent increasing distance from the hot spot at the time of crustal formation and infer the following scenario. When the Siletz terrane collided with the North American continent approximately 50 Ma, the thickened oceanic crust was too buoyant to be subducted and was instead accreted to the continent, causing a dramatic westward jump of the subduction zone and nearly eliminating a large embayment in the western margin of North America (29). Some normal- and transitional-thickness oceanic crust was also accreted to the forearc during this process, resulting in the observed along-strike variations in the thickness and width of the Siletz terrane (Fig. 5C). These variations are correlated with a variety of other geologic and geophysical observations.

Seismicity is relatively high in both the

overriding North American and underthrust Juan de Fuca–Gorda plates in northwestern Washington, where the Siletz terrane is thinner, and in northern California, where the Siletz terrane is absent and the forearc is floored by the Paleozoic age Klamath block (2, 30). Forearc seismicity is lowest where the Siletz terrane is thickest. The magnitude 5.6 Scotts Mills earthquake (31), which occurred in March 1993 about 50 km south of Portland, Oregon, along the northwest-trending Mount Angel fault zone, may have occurred along the transition between the thickest part of the Siletz terrane and Siletz basement of transitional thickness.

This pattern of variation in the amount of internal deformation of the Siletz terrane appears to have been present since its accretion. Paleomagnetic measurements indicate that in western Oregon the Siletz terrane has acted as a single block since accretion, whereas in southwestern Washington it has been broken into several coherent blocks that have rotated relative to one another (32) and are separated by zones of higher seismicity and crustal conductivity (33). The greatest amount of deformation is observed in northwest Washington, where geologic mapping shows that the Siletz terrane (9) has been deformed into a broad

anticline with steeply dipping limbs that wrap around the younger Olympic accretionary complex in northwestern Washington (34). Beneath Vancouver Island, the Siletz terrane has been deeply subducted. These observations suggest that the crust is strongest and most buoyant where the Siletz terrane is thickest.

The thickness of the Siletz terrane is also correlated with along-strike variations in the width of the subduction complex found seaward of the Siletz terrane (Fig. 5C). The subduction complex is wider by a factor of 3 offshore southern Washington, compared with offshore central Oregon, and wider by a factor of 5 in northern Washington, where it has been uplifted and exposed on the Olympic peninsula. This observation seems incompatible with Fig. 5, A and B, which suggest more sediment subduction beneath Vancouver than beneath Oregon. We speculate that this apparent paradox may result in part from three-dimensional deformation within the subduction complex that is related to backstop geometry (35). The subduction complex appears to be partially decoupled from the rest of the forearc in that folds and faults overlie the seaward edge of the Siletz terrane and northwest-southeast-trending left-lateral

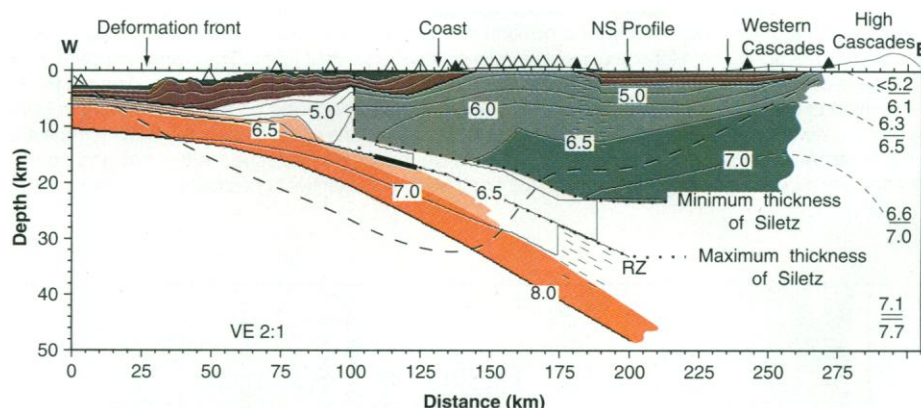


Fig. 4. Velocity model of the crust beneath the EW (east-west) profile. Contours are labeled in units of kilometers per second, and the contour interval is 0.5 km/s. The overall rms misfit of the model is 0.18 s. Open triangles show positions of offshore and onshore seismometers in 1989, resulting in 16 receiver gathers with trace spacings of 66 to 132 m; filled triangles show shot point positions in 1991, yielding four shot gathers with a 350-m trace spacing. The portion of the model constrained by observations from the 1989 and 1991 EW profiles is outlined by the light dashed line. The numbers along the eastern edge of the model indicate velocities above and below horizontal discontinuities in the model of Leaver *et al.* (26) for the velocity structure beneath the High Cascades. The position of a deep reflection beneath the continental shelf interpreted to indicate either the base of the Siletz terrane or the top of subducted oceanic crust is shown by a bold line. The projected position of crustal reflective zones onshore (16) is labeled RZ. The inferred seaward edge of the Siletz terrane and an observed fault in the overlying sediments is shown by the bold dashed line. The inferred minimum and maximum thicknesses of the Siletz terrane are shown as dotted lines. Neogene sedimentary basins with velocity less than 2 km/s are black. Sedimentary basins with velocity of 2 to 4 km/s are brown. Our interpretation of the upper and lower crust of the Siletz terrane is shown as light and dark green, respectively. The upper and lower oceanic crust of the Juan de Fuca plate are shown by light and dark orange, respectively. The apparent thickening of the upper crust beneath the lower slope is a robust feature of the model and may represent incorporation of a block of upper oceanic crust into the accretionary prism. The fate of the upper oceanic crust east of this region is uncertain (22). Small discrepancies between this model and the model of Fig. 2 at the intersection of the two profiles may reflect velocity anisotropy as well as uncertainties in the models. Cusps on the 6.5-km/s contour that approximately define the boundary between upper and lower crust are artifacts of the model parameterization. Our new model extends from km 0 to km 275.

strike-slip faults (36) extend from seaward of the deformation front to the continental shelf. These structures indicate active east-west shortening and north-south extension of the subduction complex offshore Oregon. This pattern of strain contrasts with north-

south compression observed onshore within the Siletz terrane (37), suggesting that the geometry of the Siletz terrane influences the stress field in the subduction complex.

The variations in forearc crustal structure shown in Fig. 4C also correspond close-

ly to segmentation of the Cascade volcanic arc inferred from along-arc variations in the volume and chemical composition of volcanism (38). Where the forearc is floored by the thickest part of the Siletz terrane and the backstop seems to inhibit sediment subduction, the adjacent modern arc is a continuous linear mafic platform punctuated by relatively small andesitic cones; to the north and to the south, the arc is dominated by silicic composite volcanoes (39). These variations have been attributed both to segmentation of the subducted plate (38) and to the influence of Basin and Range extension (29, 40). While Basin and Range extension is probably the primary factor affecting this pattern, variations in forearc crustal structure and backstop configuration may also influence arc magmatism by controlling the amount of oceanic crust, sediment, and water that are subducted to great depth.

These proposed explanations for the observed correlations and implications of these velocity models for estimates of seismic hazard must now be explored quantitatively through thermal and mechanical modeling of subduction zone behavior with realistic rheological and geometrical parameters derived from the velocity models. We speculate that the large variability in the material properties of the forearc implies variability in the properties of the interface between the Juan de Fuca-Gorda and North American plates, limiting the maximum size of interplate earthquakes.

Conclusions

We have presented a model for the velocity structure of the Cascadia forearc beneath northwestern Oregon that reveals considerable variability within the crust of the forearc. Observed correlations between the thickness of the Siletz terrane and both long- and short-term measures of forearc deformation suggest that the strength of the crust increases with the thickness of the Siletz terrane, providing a physical basis for the observed historical distribution of seismicity within the North American plate through the relation between crustal velocity, composition, and rheology. Correlations between crustal structure, deformation within the subduction complex, and arc magmatism indicate that variations in backstop geometry along an arc may be an important factor controlling both along-strike and down-dip transport of material within the subduction complex. These results underscore the relation between crustal architecture and geodynamic processes in subduction zones and indicate that forearc crustal structure needs to be considered when interpreting variations in arc magmatism and forearc deformation in other regions.

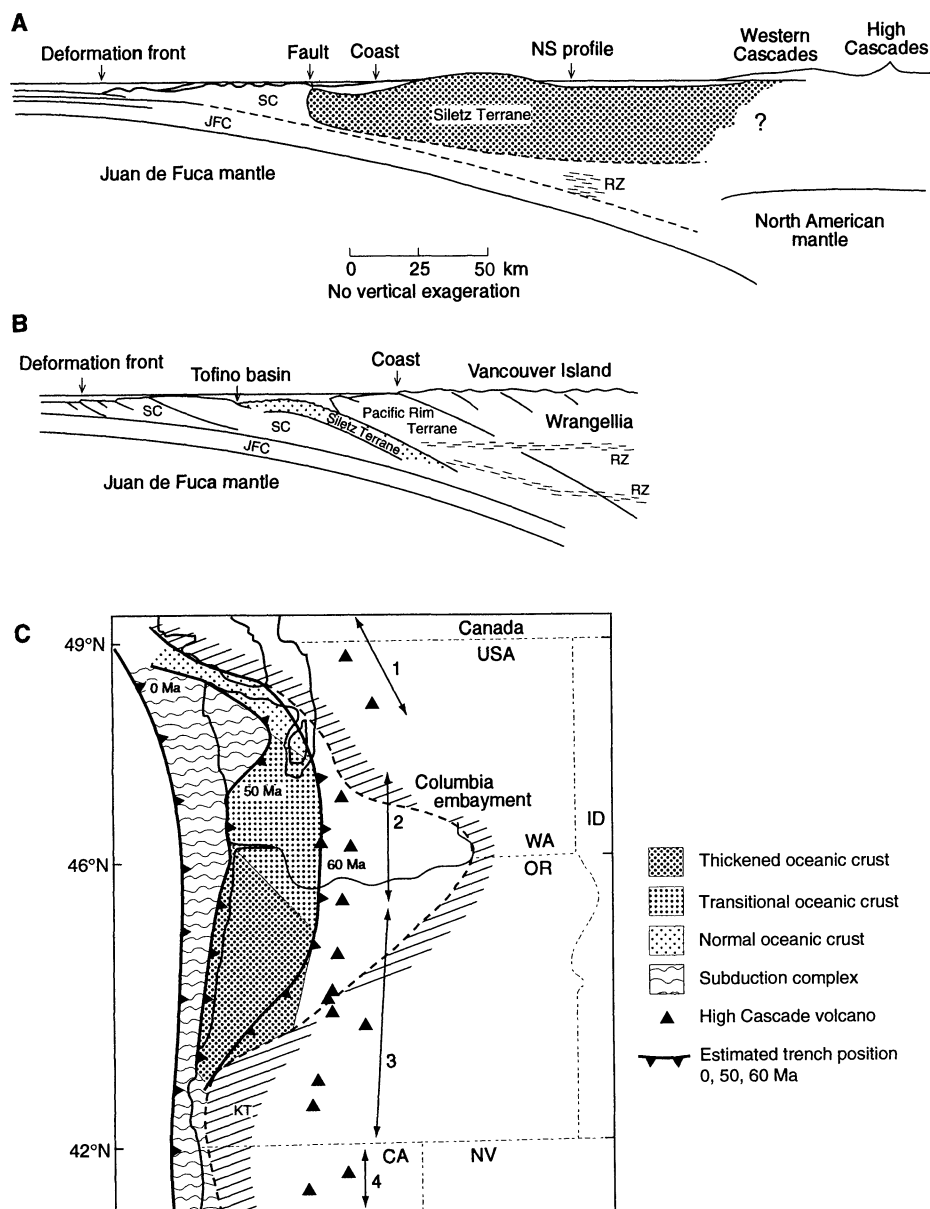


Fig. 5. (A) Summary of our model of the Cascadia forearc in Oregon, shown with no vertical exaggeration. In addition to the data discussed above, this figure includes an approximate estimate of the position of the Juan de Fuca plate crust within the upper mantle beneath the eastern Willamette Valley derived from the 1993 broadband teleseismic array experiment (8). SC, subduction complex; JFC, oceanic crust of the Juan de Fuca plate; RZ, reflective zone. (B) Crustal structure of the Cascadia forearc beneath Vancouver Island derived from a multidisciplinary synthesis of various types of geophysical data and discussed in detail by R. Hyndman *et al.* (5). Abbreviations and scale are the same as in (A). The Pacific Rim and Wrangellia terranes are of pre-Tertiary age. (C) Map of the Pacific Northwest showing regional variations in the thickness of the Siletz terrane. Numbers next to arrows show the segmentation of the volcanic arc (38). This figure shows the minimum extent of the Siletz terrane because its eastern boundary may extend farther east beneath the Cascades, its western boundary may have been truncated through strike-slip motion (12), and its southern boundary may extend beneath the Paleozoic rocks of the Klamath terrane (KT). The orientation of the boundary between thickened oceanic crust and transitional oceanic crust is poorly constrained and is shown here to be approximately coincident with the Mount Angel-Gales Creek fault zone because it occurs near this fault zone on the NS profile. The detailed location of the boundary between transitional and normal oceanic crust is also poorly known.

REFERENCES AND NOTES

1. The offshore deformation front associated with the Cascade subduction zone was first recognized by E. Silver [*Mar. Geol.* **13**, 239 (1972)].
2. The anomalously low level of seismicity in the Pacific Northwest was first noted by T. Heaton and H. Kanamori [*Bull. Seismol. Soc. Am.* **74**, 933 (1984)] and has been discussed in many subsequent papers. For a review, see K. Shedlock and C. Weaver, *U.S. Geol. Surv. Circ.* 1067 (1991).
3. Examples are B. F. Atwater and D. K. Yamaguchi, *Geology* **19**, 706 (1991); and M. E. Darienzo and C. D. Peterson, *Tectonics* **9**, 1 (1990).
4. Examples are C. A. Michaelson and C. S. Weaver, *J. Geophys. Res.* **91**, 2077 (1986); J. Rasmussen and E. Humphries, *Geophys. Res. Lett.* **15**, 1417 (1988); and R. Harris, H. Iyer, P. Dawson, *J. Geophys. Res.* **96**, 19879, (1991).
5. R. D. Hyndman and K. Wang, *J. Geophys. Res.* **98**, 2039, (1993).
6. R. Hyndman *et al.* [*Can. J. Earth Sci.* **27**, 313 (1989)] summarize the results of many years of multidisciplinary studies of the Cascadia subduction zone beneath Vancouver Island and the adjacent continental margin by the Geological Survey of Canada and university colleagues.
7. The 1989 experiment comprised an offshore multichannel seismic-reflection profile obtained with a large-volume tuned airgun source and long streamer; the airgun shots were also recorded by ocean bottom and onshore seismometers to provide complementary large-aperture data. In 1991, this study was extended into the foothills of the Cascades with several hundred seismometers and large explosive shots onshore. In 1993, broadband seismometers were deployed in an array extending from the coast into the backarc region to record teleseismic earthquakes, thereby extending the depth and breadth of coverage and providing constraints on shear wave velocities. Processing and interpretation of the multichannel seismic data are discussed in detail by A. Trehu *et al.* (in preparation). The ocean bottom seismometer data are in A. Trehu and Y. Nakamura, *U.S. Geol. Surv. Open-File Rep.* 93-317 (1993). The onshore recordings of offshore shots are in T. Brocher, M. Moses, A. Trehu, *ibid.*, 93-318 (1993). The 1991 data are in A. Trehu *et al.*, *ibid.*, 93-319 (1993); and J. Luetgert *et al.*, *ibid.*, 93-347 (1993). The broadband experiment is discussed by J. Nabelek *et al.*, *Eos* **74** (fall meeting suppl.), 431 (1993).
8. We used a hybrid forward-inverse modeling procedure (A. Trehu, in preparation; K. Blair and A. Trehu, in preparation) based on the ray-tracing, travel-time inversion, and ray-synthetic seismogram calculation techniques of C. Zelt and R. Smith [*Geophys. J. Int.* **108**, 16 (1992)]. For the NS profile, the crust was divided into layers of constant thickness with velocities specified at the top and bottom of each layer. Velocities providing the best fit to the observed travel times were determined through least squares inversion. The final model was determined by gradually increasing the number of velocity nodes in a given layer until additional nodes did not significantly improve model fit as indicated by an *F* test. The number of nodes per layer ranged from 15 in the upper crust to 4 in the mid- and lower crust. A similar procedure was used for the EW profile, although layers were not specified to be of constant thickness because of the inherent asymmetry of the structure. The water depth, shallow basin structure, and top of the subducted oceanic crust were constrained by the coincident seismic reflection data. For the initial inversion, the sub-basement structure was represented by a single layer of laterally variable velocity. Additional complexity was allowed in the model after detailed examination of the best fitting solution for a given model parameterization. The velocity models thus derived are generally compatible with the coincident potential field data.
9. In west-central Oregon, these rocks are known as the Siletz terrane and are described by P. Snively Jr. *et al.* [*Am. J. Sci.* **266**, 454 (1968)]; in southwestern Oregon, they are known as the Roseburg terrane; in southwestern Washington, they are known as the Gray's Harbor terrane; in northwestern Washington, they are known as the Crescent terrane (R. W. Tabor and W. M. Cady, *U.S. Geol. Surv. Map I-994*, 1978); and on Vancouver Island, they are known as the Metochosin Formation.
10. R. A. Duncan, *J. Geophys. Res.* **87**, 827 (1982).
11. R. E. Wells *et al.*, *Tectonics* **3**, 275 (1984).
12. P. Snively Jr., in *Geology and Resource Potential of the Continental Margin of Western North America and Adjacent Ocean Basins—Beaufort Sea to Baja California* (Circum-Pacific Council for Energy and Mineral Resources, Houston, TX, 1987), vol. 6, p. 305.
13. C. Finn, *J. Geophys. Res.* **95**, 19533 (1990).
14. R. J. Blakely, *ibid.* **99**, 2757 (1994).
15. J. L. Nabelek and X.-Q. Li, unpublished data.
16. D. M. Hussong, L. K. Wiperman, and L. W. Kroeke [*J. Geophys. Res.* **84**, 6003 (1979)] determined that the Ontong-Java plateau has a 10-km-thick upper crust with a velocity of 5.4 to 6.1 km/s underlain by a 26-km-thick lower crust with velocity of 6.9 to 7.6 km/s. In their study, which included several other oceanic plateaus in the Pacific, they derived a constant of proportionality of 0.3 to 0.4 relating the thickness of oceanic "layer 2," as defined by velocities below 6.5 km/s, to the total oceanic crustal thickness. In a global review of oceanic crustal structure, C. Z. Mutter and J. C. Mutter [*Earth Planet. Sci. Lett.* **117**, 295 (1993)] confirm that the thickness of oceanic layer 2 increases systematically as the total crustal thickness increases but question whether this relation can be simply described by a constant.
17. The conclusion that the Juan de Fuca plate–North American plate boundary is within the lower crust beneath the NS profile is supported by eastward extrapolation of the EW profile and by the absence in the teleseismic receiver function from Corvallis, OR, of signals that would be expected if a layer of subducted Juan de Fuca crust were embedded in the underlying mantle (15). Such a signal is found farther east in data from the 1993 broadband array (7).
18. The interpretation of a thick oceanic plateau-like terrane overlying a heterogeneous lower crust is supported by four additional seismological observations. First, the simple wavelet of the first arriving energy along the NS profile contrasts markedly with the complicated wave forms observed in southeast Alaska [G. S. Fuis *et al.*, *J. Geophys. Res.* **96**, 4187 (1991)] and modeled as a stack of imbricated oceanic crustal layers [E. Flueh *et al.*, *ibid.* **94**, 16023 (1989)]; this observation, combined with the upper crustal velocity gradient, indicates a thick oceanic plateau rather than imbricated oceanic crust for the upper 25 km of our model. Second, the receiver function analysis from Corvallis, OR (15), indicates that the average Poisson's ratio for the crust is 0.33, suggesting a dominantly mafic composition for the entire crustal column. Third, a short seismic reflection profile that intersects our model near km 290 [R. W. Keach *et al.*, *Geol. Soc. Am. Bull.* **101**, 339 (1989)] indicates that the upper crust is highly reflective (consistent with oceanic layer 2), that the mid-crust is transparent (consistent with lower oceanic crust), and that the lower crust is again reflective (consistent with a heterogeneous zone of tectonically or magmatically underplated material). Fourth, pre-critical reflections from depths of 35 to 40 km beneath the NS profile are observed from several of the 1991 shot points (K. Blair and A. Trehu, in preparation).
19. Lithospheric cross sections across the Cascadia subduction zone in Oregon can be found in review papers [R. Couch and R. Riddiough, *Geol. Soc. Am. Mem.* **172**, 103 (1989); W. Mooney and C. Weaver, *ibid.*, p. 129; R. Duncan and L. Kulm, in *The Geology of North America*, vol. N, *The Eastern Pacific Ocean and Hawaii* (Geological Society of America, Boulder, CO, 1989), ch. 22]. Large differences among these cross sections are due to limitations of the data available at the time.
20. P. Wannamaker *et al.*, *J. Geophys. Res.* **94**, 127 (1989).
21. Details of the structure in this region are discussed by M. Mackay *et al.* [*Earth Planet. Sci. Lett.* **109**, 477 (1992)].
22. We suspect that our inability to image the subducted crust beneath the continental slope in the seismic reflection data is due to scattering because of the presence of gas combined with heterogeneous structure within the subduction complex. The large-aperture data permit us to delineate the lower oceanic crust because of its characteristic seismic velocity of 6.8 to 7.2 km/s. We are not able to unambiguously distinguish upper oceanic crust, which generally has a velocity less than 4 km/s at the sea floor, increasing to about 6.5 km/s at a depth of 2 km. Therefore, the velocity of upper oceanic crustal velocities is similar to that of deeply buried accreted sediments; alternatively, its velocity may increase with burial because of closing of cracks and be similar to that of lower oceanic crust. This ambiguity concerning the velocity of deeply subducted upper oceanic crust should not be a significant factor when interpreting the velocity structure of the Siletz terrane (16, 18) because the thickest parts of the Siletz terrane were probably never deeply subducted and because the pervasive cracking resulting from hydrothermal circulation, which greatly lowers the in situ velocity of the uppermost oceanic crust, probably did not extend to the base of the overthickened upper oceanic crust.
23. In the "bulldozer" model of subduction of W. M. Chapple [*Geol. Soc. Am. Bull.* **89**, 1189 (1978)] and D. Davis, J. Suppe, and F. A. Dahlen [*J. Geophys. Res.* **88**, 1153 (1983)], the backstop is a rigid buttress that moves relative to the subducting plate, deforming the sediments on the subducting plate into a wedge with a steady-state geometry that is controlled by the internal friction of the wedge and the basal friction on the plate interface.
24. P. Snively Jr., H. C. Wagner, D. L. Lander, *Geol. Soc. Am. Map Chart Ser. MC-28J* (1980).
25. The depth and eastward extent of this low-velocity region corresponds very closely to a low-conductivity anomaly region in the EMSLAB model (20). The low conductivity beneath the Cascades was interpreted to be associated with exposed volcanic rocks, which dip to the east. Because the velocity in this region is significantly lower than that of the near-surface Cascade volcanic rocks and indistinguishable from that of the rocks in the Willamette Valley, we believe that this material is predominantly sedimentary rocks. Geologic observations near Roseburg support this interpretation [G. Walker and N. S. Macleod, *Geologic Map of Oregon* (U.S. Geological Survey, 1991); R. Wells, personal communication (1992)].
26. D. S. Leaver, W. D. Mooney, W. M. Kohler, *J. Geophys. Res.* **89**, 3121 (1984).
27. A pronounced arch in the plate was inferred by R. S. Crosson and T. J. Owens [*Geophys. Res. Lett.* **14**, 824 (1987)], who assumed a dip of 20° when contouring the base of the subducted Juan de Fuca plate beneath the Pacific Northwest. If one revises their contours to be consistent with our model, the apparent arch in the plate is greatly reduced.
28. M. A. Richards, R. A. Duncan, V. E. Courtillot, *Science* **246**, 103 (1989); R. S. White and D. P. McKenzie, *J. Geophys. Res.* **94**, 7685 (1989).
29. Figure 5C incorporates information from S. Hughes, *J. Geophys. Res.* **95**, 19623 (1990). The approximate western limit of pre-Tertiary crust as observed on the surface is labeled "Columbia Embayment" and is taken from W. Hamilton and W. B. Myers, *Rev. Geophys.* **4**, 509 (1966). Although this embayment in the North American craton has a very large curvature, much of the curvature may be due to Tertiary Basin and Range extension [see R. E. Wells and P. L. Heller, *Geol. Soc. Am. Bull.* **100**, 325 (1988)]. The estimated position of the trench at 60 Ma is from W. R. Dickinson, in *Cenozoic Paleogeography of Western United States*, J. M. Armentrout, M. R. Cole, H. Terbest Jr., Eds. (Society of Economic Paleontologists and Mineralogists, Los Angeles, 1979), pp. 1–13. The subsurface western limit of pre-Tertiary crust probably lies between these two boundaries. The estimated position of the trench at 50 Ma corresponds to the western edge of the Siletz terrane, on the basis of magnetic anomalies.
30. R. Wells and C. Weaver, *U.S. Geol. Surv. Open-File Rep.* 93-333 (1993) p. 14.
31. I. Madin *et al.*, *Oreg. Geol.* **55**, 51 (1993).
32. R. Wells, *J. Geophys. Res.* **95**, 19409 (1990).
33. G. Egbert and J. Booker, *ibid.* **98**, 15967 (1993).

34. M. Brandon and J. Vance, *Am. J. Sci.* **292**, 565 (1992).
35. Other factors that must be considered when reconstructing the long-term mass balance within the subduction complex include the oblique component of relative plate motion (Fig. 1), which may result in lateral material transport along north-south-trending strike-slip faults (12) and variable sediment input to the accretionary wedge due to the presence of large sedimentary fans offshore Washington and northern Oregon.
36. C. Goldfinger *et al.*, *Geology* **20**, 141 (1992).
37. K. Werner *et al.*, *Tectonics* **10**, 948 (1991).
38. M. Guffanti and C. S. Weaver, *J. Geophys. Res.* **93**, 6513 (1988).
39. D. Sherrod and J. Smith, *ibid.* **95**, 19465 (1990).
40. M. Guffanti *et al.*, *ibid.*, p. 19453; S. Hughes, *ibid.*, p. 19623.
41. C. DeMets *et al.*, *Geophys. J. Int.* **101**, 425 (1990).
42. We thank the many people who participated in the permitting, data acquisition, and processing phases of these experiments. Comments from M. Fisher, S.

Guest, A. Jones, K. Rohr, and R. Wells greatly improved the manuscript. This work was supported by grants from NSF (OCE-8900962 and EAR-8905189 to A.M.T.) and by the U.S. Geological Survey (USGS) internal and external National Earthquake Hazards Reduction Program. Seismic instrumentation was provided by the USGS, the University of Texas at Austin, the Geological Survey of Canada, Stanford University, and the NSF IRIS/PASSCAL program. This is Geological Survey of Canada contribution number 21594.

RESEARCH ARTICLE

A Designed Peptide Ligase for Total Synthesis of Ribonuclease A with Unnatural Catalytic Residues

David Y. Jackson,* John Burnier, Clifford Quan, Mark Stanley, Jeffrey Tom, James A. Wells†

An engineered variant of subtilisin BPN', termed subtiligase, which efficiently ligates esterified peptides in aqueous solution, was used for the complete synthesis of ribonuclease (RNase) A that contains unnatural catalytic residues. Fully active RNase A (124 residues long) was produced in milligram quantities by stepwise ligation of six esterified peptide fragments (each 12 to 30 residues long) at yields averaging 70 percent per ligation. Variants of RNase A were produced in which the catalytic histidines at positions 12 and 119 were substituted with the unnatural amino acid 4-fluorohistidine, which has a pK_a of 3.5 compared to 6.8 for histidine. Large changes in the profile of the pH as it affects rate occurred for the single and double mutants with surprisingly little change in the k_{cat} for either the RNA cleavage or hydrolysis steps. The data indicate that these imidazoles function as general acids and bases, but that the proton transfer steps are not rate-limiting when the imidazoles are present in their correct protonation states. These studies indicate the potential of subtiligase for the blockwise synthesis of large proteins.

Engineering proteins is usually limited to the application of mutagenesis and recombinant expression technologies. The ability to probe and alter protein function would be greatly expanded by generic methods to incorporate unnatural amino acids or other structures, which would allow much greater diversity and precision in protein design. However, chemical synthesis has largely been restricted to small peptides (typically less than 40 residues in length) because of the accumulation of side products that complicate product purification and decrease yields (1, 2). Alternatively, coupling synthetic peptide fragments by selective chemical (3–6) or enzymatic methods (7–11) suggests that routine synthesis of proteins

more than 100 residues long in high purity and good yield may soon be within reach.

Progress has been made in engineering the bacterial serine protease, subtilisin BPN', for catalyzing peptide bond formation in aqueous solution (9–11). The most efficient variant (11), termed subtiligase, is a double mutant in which the catalytic Ser²²¹ is converted to Cys, and Pro²²⁵ is mutated to Ala (S221C and P225A) (12). The S221C mutation increases the aminolysis to hydrolysis ratio of tetrapeptide esters (9, 13) while the P225A mutation improves catalytic activity by reducing steric crowding in the active site caused by S221C. The k_{cat} value for subtiligase catalyzed aminolysis of a good peptide ester is comparable to the hydrolysis of analogous amide substrate by wild-type subtilisin (20 s^{-1} compared to 50 s^{-1}). Although this enzyme showed promise in single couplings of short peptide esters (11), it had not been shown to be useful for sequential couplings with long peptides.

We now describe a practical coupling

and deprotection strategy that allows subtiligase to be used for the blockwise assembly of proteins. For our model synthetic protein we chose ribonuclease (RNase) A, a 124-residue enzyme, because of its interesting catalytic mechanism (14) and established crystal (15) and solution structures (16). The enzyme can be refolded (17, 18) and easily assayed (19, 20). Furthermore, RNase A has been synthesized earlier (5, 21), albeit in low yield and moderate purity. The blockwise enzymatic synthesis of RNase A allowed us to produce the enzyme in higher yield and purity. As a result we were able to incorporate unnatural catalytic residues that alter the catalytic properties so that the enzyme mechanism could be probed in more detail that was not possible with conventional site-directed mutagenesis.

Synthesis of RNase A and variants containing 4-fluorohistidine. The strategy for protein synthesis with subtiligase (Fig. 1) starts with preparation of a fully deprotected peptide (the acceptor) that corresponds to the COOH-terminal fragment of the desired protein. The next most NH₂-terminal fragment (the donor) is esterified with glycolate-phenylalanyl amide (glc-F-NH₂) on the COOH-terminus. This ester efficiently acylates subtiligase because the enzyme has a preference for esters containing the glc-F-NH₂ leaving group (11). The donor fragment also contains an isonicotinyl (iNOC) protecting group (22) on its NH₂-terminus to prevent self ligation (Fig. 1). The iNOC group can be incorporated at the last step of solid phase peptide synthesis and is stable to anhydrous hydrofluoric acid, which is used to deprotect side chains and cleave peptides from the solid phase resin. After each ligation the iNOC group can be removed from the peptide under mild reducing conditions (Zn(s) and acetic acid) to generate the free NH₂-terminus for subsequent ligations.

We divided RNase A into six peptide fragments (Table 1) based on the substrate specificity of subtiligase (11, 23). Subtiligase is efficient with large and hydrophobic P1 donor substrates and inefficient with negatively charged residues or Pro at P1' (24). The peptides were synthesized (25) and ligated together in a sequential manner (26). The average yield was 66 percent per coupling step and 86 percent per deprotection step.

D. Y. Jackson and J. A. Wells are in the Department of Protein Engineering and J. Burnier, C. Quan, M. Stanley, and J. Tom are in the Department of Bioorganic Chemistry, Genentech, Inc., 460 Point San Bruno Boulevard, South San Francisco, CA 94080, USA.

*Present address: Department of Bioorganic Chemistry, Genentech, Inc., San Francisco, CA 94080, USA.

†To whom correspondence should be addressed.

LINKED CITATIONS

- Page 1 of 1 -



You have printed the following article:

Crustal Architecture of the Cascadia Forearc

A. M. Trehu; I. Asudeh; T. M. Brocher; J. H. Luetgert; W. D. Mooney; J. L. Nabelek; Y. Nakamura

Science, New Series, Vol. 266, No. 5183. (Oct. 14, 1994), pp. 237-243.

Stable URL:

<http://links.jstor.org/sici?sici=0036-8075%2819941014%293%3A266%3A5183%3C237%3ACAOTCF%3E2.0.CO%3B2-S>

This article references the following linked citations. If you are trying to access articles from an off-campus location, you may be required to first logon via your library web site to access JSTOR. Please visit your library's website or contact a librarian to learn about options for remote access to JSTOR.

References and Notes

²⁸ **Flood Basalts and Hot-Spot Tracks: Plume Heads and Tails**

Mark A. Richards; Robert A. Duncan; Vincent E. Courtillot

Science, New Series, Vol. 246, No. 4926. (Oct. 6, 1989), pp. 103-107.

Stable URL:

<http://links.jstor.org/sici?sici=0036-8075%2819891006%293%3A246%3A4926%3C103%3AFBAHTP%3E2.0.CO%3B2-W>

NOTE: *The reference numbering from the original has been maintained in this citation list.*